

# Electric-field coupling to spin waves in a centrosymmetric ferrite

Xufeng Zhang,<sup>1</sup> Tianyu Liu,<sup>2</sup> Michael E. Flatté,<sup>2,\*</sup> and Hong X. Tang<sup>1,†</sup>

<sup>1</sup>*Department of Electrical Engineering, Yale University,  
15 Prospect St., New Haven, Connecticut 06511, USA*

<sup>2</sup>*Optical Science and Technology Center and Department of Physics and Astronomy,  
University of Iowa, Iowa City, Iowa 52242, USA*

(Dated: June 17, 2014)

We experimentally demonstrate that the spin-orbit interaction can be utilized for direct electric-field tuning of the propagation of spin waves in a single-crystal yttrium iron garnet magnonic waveguide. Magnetoelectric coupling not due to the spin-orbit interaction, and hence an order of magnitude weaker, leads to electric-field modification of the spin-wave velocity for waveguide geometries where the spin-orbit interaction will not contribute. A theory of the phase shift, validated by the experiment data, shows that, in the exchange spin wave regime, this electric tuning can have high efficiency. Our findings point to an important avenue for manipulating spin waves and developing electrically tunable magnonic devices.

PACS numbers: 75.30.Ds, 75.70.Tj, 75.85.+t, 85.75.-d

Interest in magnonics, which focuses on collective spin currents, originates from the greater stability of the collective motion of spins (spin waves); their persistence for longer distances and consumption of less energy compared to spin-polarized current makes magnonics competitive for low loss integrated spintronics [1–4]. Particularly, the interaction between an electric field and a spin wave provides fundamental insight into the coupling between charge and spin degrees of freedom in a solid. Detection of this interaction at room temperature in single-crystal yttrium iron garnet ( $\text{Y}_3\text{Fe}_5\text{O}_{12}$ , YIG), a material of great interest for magnonic device design because of its exceptionally low damping rate for spin waves [5] and rich linear and nonlinear properties [6–14], has proved difficult due to the lack of spontaneous electric polarization in YIG [15]. The presence of a center of inversion symmetry in single-crystal YIG prevents it from responding to applied electric fields via the same mechanism as materials such as frustrated magnets or multiferroics [16–19]. So far only indirect electric tuning of YIG has been achieved, with the assistance of piezoelectric materials [20–23].

In this Letter, we demonstrate direct electric field control of spin waves in a YIG magnonic waveguide via a predicted, but not previously observed, mechanism that occurs even in materials with a center of inversion symmetry. Our analysis shows that this effect mostly stems from a spin-orbit (SO) interaction with a minor contribution from a first-order magnetoelectric (ME) effect. The SO interaction has recently attracted intense interest because it provides new approaches for manipulating electron spins [24]. In ferromagnets it leads spin waves that propagate in an applied electric field to acquire an Aharonov-Casher (AC) phase [25]. To linear order of the electric field this is equivalent to adding a Dzyaloshinskii-Moriya-like (DM-like) interaction between neighboring spins ( $\mathbf{S}_{i,j}$ ) that takes the form [26, 27]:  $H_{ij} = \mathbf{D}_{ij} \cdot (\mathbf{S}_i \times \mathbf{S}_j)$ , where  $|\mathbf{D}| \propto E/E_{\text{SO}} = 2m\lambda_{\text{SO}}^2 E/\hbar^2$  is the DM vector,  $m$  is the electron rest mass,  $\hbar$  is the reduced

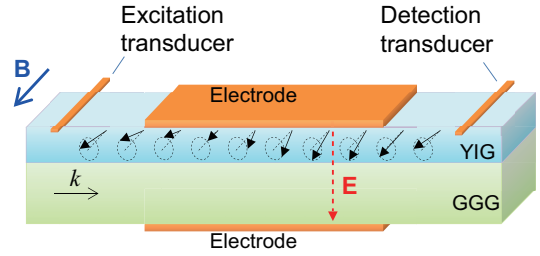


Figure 1. (Color online). Schematic of the YIG magnonic waveguide used in this experiment.  $B$ : bias magnetic field;  $E$ : electric field;  $k$ : wave vector.

Planck constant, and  $\lambda_{\text{SO}}$  is a characteristic length scale that determines the SO interaction strength. Through this effect the applied electric field adds an AC phase to the spin waves [25, 28–30]. The SO interaction in YIG was previously considered to be extremely small due to an assumption that  $\lambda_{\text{SO}} = \lambda_c$  (the reduced Compton wavelength). A recent theoretical study predicts that the SO interaction can be orders of magnitude larger in YIG if one considers orbital hybridization, which yields  $\lambda_{\text{SO}} \gg \lambda_c$  [31, 32]. Here we present experimental observation of this SO interaction in a single-crystal YIG thin film. In addition, our experiments found an electric tuning of the ferromagnetic resonance (FMR) frequency which we attribute to a first-order ME effect. Noting that the SO interaction depends on an orthogonality between the applied electric field, the equilibrium magnetization and the wave vector of the spin waves, while the ME effect does not, we clearly identify the different contributions from the two effects by applying the electric field out-of-plane and in-plane.

Figure 1 shows the schematic of our device, containing a narrow strip of YIG thin film as the magnonic waveguide, a pair of copper electrodes to apply electric fields across the waveguide, and a pair of microstrip transducers to excite and detect the spin waves. The YIG strip (2

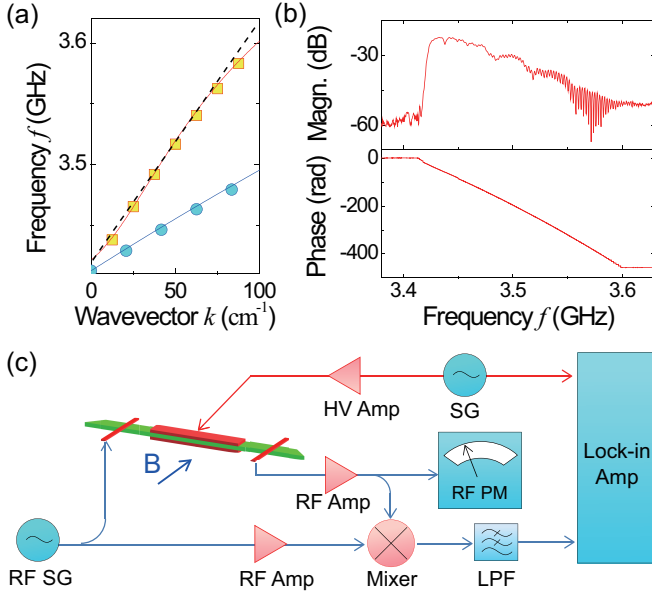


Figure 2. (Color online). (a) Dispersion relation of the spin wave in the YIG magnonic waveguide. Red squares and blue circles are the experimentally extracted dispersions with and without metal electrodes on the YIG surface, respectively. Solid lines are the theoretical calculations. Dashed black line is the linearized dispersion. (b) Vector network analyzer transmission characterization of the YIG magnonic waveguide with magnitude response shown in the top panel and phase response shown in bottom panel. (c) Interferometry scheme for measuring spin wave phase accumulation. SG: signal generator; RF SG: radio frequency signal generator; Amp: amplifier; PM: powermeter; LPF: low-pass filter; HV Amp: high voltage amplifier.

mm  $\times$  40 mm) is cut from a 5- $\mu$ m-thick thin film of single-crystal YIG epitaxially grown on a 0.5-mm-thick gadolinium gallium garnet (Gd<sub>3</sub>Ga<sub>5</sub>O<sub>12</sub>, GGG) substrate. To avoid magnon reflection, the two ends of the YIG strip are terminated by 45° angled cuts. The two microstrip transducers are placed 30 mm apart over the two ends of the magnonic waveguide. The excited spin waves propagate along the long axis of the magnonic waveguide. The electrodes are attached onto the top and bottom surfaces of the device and cover 20 mm length of the waveguide to provide a sufficiently long interaction length. This leaves a 5 mm gap between the electrode and the microstrip transducer which is wide enough to avoid electrical cross-talk between transducers. As the SO interaction requires the wave vector  $\mathbf{k}$ , the magnetization  $\mathbf{M}$  and the electric field  $\mathbf{E}$  to be orthogonal, we apply the bias magnetic field in-plane and transverse to the wave propagation direction.

In this configuration the excited spin wave mode in the magnonic waveguide is a magnetostatic surface spin wave (MSSW). Using methods provided in Refs. [33] and [34], we calculate the dispersion of the MSSW taking into

account the effects of the GGG substrate and electrodes:

$$e^{2kd} = \frac{1 - \chi + \kappa - \tanh(kt_1)}{1 - \chi - \kappa + \tanh(kt_1)} \cdot \frac{1 - \chi - \kappa - \tanh(kt_2)}{1 - \chi + \kappa + \tanh(kt_2)}, \quad (1)$$

where  $\chi = \frac{f_B f_M}{f_B^2 - f^2}$  and  $\kappa = \frac{f f_M}{f_B^2 - f^2}$  with  $f$  being the frequency,  $f_B = \gamma B$ ,  $f_M = 4\pi\gamma M_0$ . Other parameters are: the bias magnetic field  $B$ , the equilibrium magnetization  $4\pi M_0$ , the gyromagnetic ratio  $\gamma$ , the wave vector  $k$ , YIG film thickness  $d$ , the gap between the YIG film and the upper (lower) electrode  $t_1$  ( $t_2$ ). Note that  $t_2$  is approximately the thickness of the GGG layer.

In Fig. 2(a) we present the calculated dispersions of the waveguide with and without electrodes using Eq. (1) (the solid red line versus the solid blue line). In both cases, the electric field is set at zero. The calculated dispersions agree well with the experimental data (circles and squares). The presence of electrodes on the YIG surface increases the group velocity of the spin waves.

For small  $k$  values (which is the case in our experiment due to the limits of the transducers), the dispersion can be linearized by expanding the original dispersion  $f = \Omega(k)$  around  $k_0$  to the first order of  $(k - k_0)$ :

$$f = \Omega_0 + v_{g0}(k - k_0) = v_{g0}k + f_{\text{FMR}}, \quad (2)$$

where  $\Omega_0 = \Omega(k_0)$ ,  $v_{g0} = \partial_k \Omega(k_0)$  is the group velocity at  $k_0$ , and  $f_{\text{FMR}}$  is the FMR frequency obtained after the linearization. The dashed line in Fig. 2(a) shows the linearized dispersion expanded around  $k_0 = 60 \text{ cm}^{-1}$  and it replicates the complete dispersion within the range  $k < 70 \text{ cm}^{-1}$ .

The spin wave propagation along the waveguide is characterized using microwave transmission measurement [Fig. 2(b)]. Under a bias magnetic field of 60.1 mT the spin wave transmission band covers 3.42 – 3.58 GHz within which the spin wave accumulates a very large phase after propagating through the waveguide owing to its small phase velocity. From the phase spectrum we extract the MSSW dispersion.

When an external electric field is applied across the magnonic waveguide as in Fig. 1, the spin wave phase accumulation is modified as a result of the SO interaction. Such phase changes can be precisely detected with our interferometry scheme [Fig. 2(c)]. One arm of the interferometer is the magnonic waveguide, whereas the other arm is a reference signal originating from the same microwave source. The power sent into the magnonic waveguide is kept below the nonlinear threshold of the MSSW to avoid undesired nonlinear effects. The electric-field-induced phase is measured by comparing these two arms at the phase detector, which consists of a mixer and a low-pass filter. The measured phase is normalized by the transmitted power and monitored by a RF powermeter to eliminate the amplitude information. To increase the measurement sensitivity and suppress system fluctuations, the applied electric field is modulated at 7 kHz and a lock-in amplifier is used to detect the corresponding phase modulation.

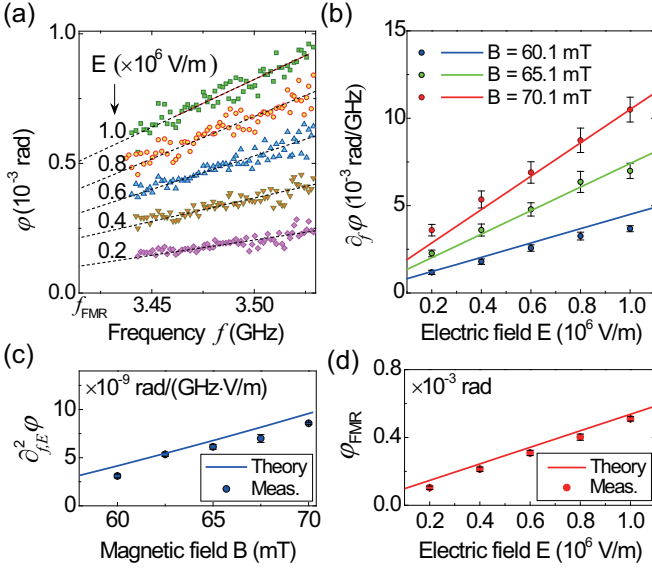


Figure 3. (Color online). (a) Measurement of the electric-field-induced phase (symbols) at various electric fields (bias magnetic field  $B = 60.1$  mT). Dashed lines show the linear fittings. (b) Dependence of  $\partial_f \varphi$  on the electric field with different bias magnetic fields. Solid lines show the theoretical predictions. (c) Dependence of  $\partial_{f,E}^2 \varphi$  on the magnetic field. (d) Phase induced by the first-order ME effect at the FMR frequency (bias magnetic field  $B = 60.1$  mT).

Figure 3(a) shows the measured phase signal induced by different electric fields with a bias magnetic field of 60.1 mT. At an applied electric field of  $\sim 10^6$  V/m, the resulting phase (normalized to the propagation distance) is of the order of  $10^{-5}$  rad/mm. We note that this value can be drastically enhanced by decreasing the wavelength. Especially, it is estimated that a  $\pi$ -phase shift can be achieved as the wavelength approaches the exchange limit [32]. The phase shift signal has a clear dependence on the electric field, demonstrating the electric tuning origin.

In the AC effect picture, the SO interaction provides an electric-field-dependent term  $f = f_M \lambda k$  to the dispersion [32], where  $\lambda = 2Ja^5 eE / \mu_0 E_{\text{SO}} \hbar^2 \gamma^2$ , with  $J$  being the exchange coefficient between neighboring lattices,  $a$  the lattice constant,  $e$  the elementary charge, and  $\mu_0$  the vacuum permeability. Since the magnetization of the YIG is not saturated under the applied magnetic field,  $J$  has a  $B$  dependence and accordingly  $\lambda$  can be expressed as  $\lambda = (\lambda_0 + \lambda_B B)E$ , where  $\lambda_0$  and  $\lambda_B$  are constants determined through the experiments. In another, equivalent, description, the spin wave gains an additional wave vector  $k_{\text{SO}}$  at a given frequency  $f$ , which yields an additional phase  $\varphi_{\text{SO}}$  after the spin wave propagates a distance  $L$ . Using the linear dispersion approximation we have:

$$\varphi_{\text{SO}} = \frac{L}{v_{g0}^2} f_M (f - f_{\text{FMR}}^0) (\lambda_0 + \lambda_B B) E, \quad (3)$$

where  $f_{\text{FMR}}^0$  denotes the FMR frequency in the absence of electric fields. This equation shows a clear linear de-

pendence of the SO-interaction-induced phase on the frequency and the electric field, in agreement with the data shown in Fig. 3(a).

However, Eq.(3) also indicates a zero phase shift at the FMR frequency, which deviates from our experimental observation. We attribute this discrepancy to a first-order ME effect, which directly modifies the equilibrium magnetization and is inherent to magnetic materials. Because of this ME effect,  $f_M$  becomes  $f_M + pE$  in the presence of an applied electric field, where  $p$  is a constant. Substituting the new expression into the linear dispersion given by Eq. (2) we have the total phase induced by both SO and ME effects:  $\varphi = \varphi_{\text{SO}} + \varphi_{\text{ME}}$ , where

$$\varphi_{\text{ME}} = \left( \frac{f - f_{\text{FMR}}^0}{v_{g0}^2} v_{g0}' + \frac{\partial_E \Omega_0 - v_{g0}' k_0}{v_{g0}} \right) L E, \quad (4)$$

where  $v_{g0}' = \partial_E v_{g0}$ . Note that due to the existence of the direct ME effect,  $v_{g0}$  becomes a function of  $E$ . From Eq. (4) we can see that there exists a nonzero phase at the FMR frequency. In addition, the ME effect also contributes a  $f$ -dependent term.

We compare our model (the solid lines) with the experiments (the dots) in Figs. 3(b)–(d) and a good agreement is achieved. The solid lines are obtained by taking into account both the SO effect and the direct ME effect. As predicted in Eqs. (3) and (4), the measured electric-field-induced phase is linear in the frequency and increases with the electric field [Fig. 3(a)]. This electric field dependence is shown in Fig. 3(b), where the partial derivative  $\partial_f \varphi$  is plotted as a function of the electric field at various bias magnetic fields. The magnetic field dependence of the second derivative of the phase ( $\partial_{f,E}^2 \varphi$ ) is plotted in Fig. 3(c). It can be seen that the effect of electric tuning can be enhanced by increasing the electric field and the bias magnetic field. Figure 3(d) shows that the induced phase at  $f_{\text{FMR}}^0$  is indeed nonzero due to the direct ME effect.

The good agreement between the theory and the experimental data supports our interpretation that the measured electric tuning originates from the combined effect of the SO and ME interaction with dominant contribution coming from the SO effect. In our model there are three unknown parameters:  $\lambda_0$ ,  $\lambda_B$ , and  $p$ , while the rest of the parameters are all known constants. From the measurement data we obtain these unknown parameters through numerical fitting:  $\lambda_0 = -1.095 \times 10^{-16} \text{ m}^2/\text{V}$ ,  $\lambda_B = 2.080 \times 10^{-15} \text{ m}^2/(\text{V} \cdot \text{T})$ , and  $p = 2.34 \times 10^{-3} \frac{\text{Hz}}{\text{V/m}}$ . At a bias magnetic field of 60.1 mT and electric field of  $1 \times 10^6$  V/m, we obtain  $\lambda = 0.15 \text{ \AA}$  and accordingly  $\lambda_{\text{SO}} = 0.45 \text{ \AA}$ , which is indeed two orders of magnitude larger than  $\lambda_c$  ( $3.85 \times 10^{-3} \text{ \AA}$ ).

To further separate the contributions to the phase shift from the SO and ME effects, we examine their dependence on the direction of the applied electric field. By moving the two electrodes to the side of the waveguide, we apply the electric field in the same direction as the magnetic field, as illustrated in the lower inset of

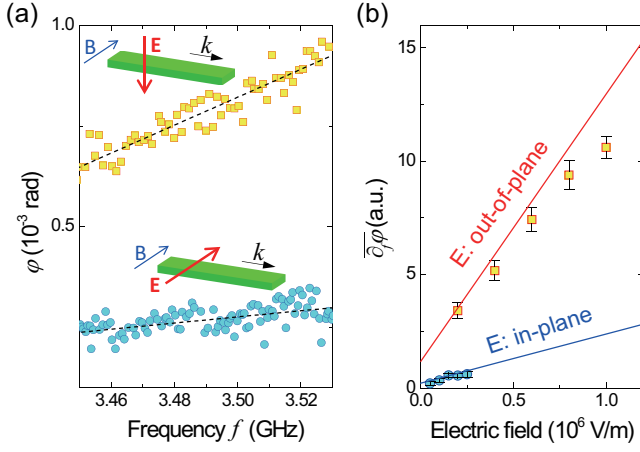


Figure 4. (Color online). (a) The measured phase shift with the electric field applied in the in-plane (blue squares) and out-of-plane (red circles) direction, respectively, under the same bias magnetic field ( $B = 60.1$  mT). Dashed black lines are the linear fittings. (b) Dependence of  $\partial\phi/\partial f$  on the electric field for the in-plane (blue circles) and out-of-plane (red squares) electric field configuration, respectively. Solid lines show the model predictions.

Fig. 4(a). The SO interaction vanishes under this configuration since it requires  $\mathbf{k}$ ,  $\mathbf{M}$  and  $\mathbf{E}$  to be all orthogonal. As the first-order ME effect does not require such orthogonality, the phase shift for this electrode configuration would arise solely from the ME effect.

Figure 4(a) compares the measured phase  $\phi$  for in-plane (circles) and out-of-plane (squares) electric fields under the same bias magnetic field ( $B = 60.1$  mT). To obtain quantitative comparison between these two curves, it is important to realize that the group velocities are different for these two cases because of the dispersion change when removing the copper electrode from the YIG surface [squares versus circles in Fig. 2(a)]. In addition, the obtainable electric field ranges are different due to the large aspect ratio of the sample cross section. Therefore it is difficult to directly compare the effects at the same electrical field. Nevertheless the change of slope or partial derivative of the phase ( $\partial_f\phi$ ) truly differentiates these two effects. In the experiments, we vary the applied electric fields and normalize the measured  $\partial_f\phi$  with the group velocity and the electric field [ $\partial_f\phi = \partial_f\phi \cdot (v_{g0}^2/E)$  in Fig. 4(b)]. The dramatically reduced slope signal indicates the greatly suppressed SO interaction for the in-plane electric field configuration. The theoretical prediction for the in-plane configuration, which only includes the ME effect using parameters obtained from the out-of-plane configuration, shows good agreement with the experiment data and validates our analysis.

In conclusion, we experimentally demonstrated the existence of the SO interaction in single-crystal YIG. Such interaction shifts the spin wave dispersion under external electric fields applied perpendicular to the magnetization and wave propagation directions. As a result,

electric-field-induced phase modulation of the propagating spin waves in a magnonic waveguide is achieved. On the other hand, we found another effect, the first-order ME effect, also contributes to the electric tuning by modifying the equilibrium magnetization with an electric field. The latter effect can be separately measured by applying the electric field in a direction parallel to the magnetization. A complete theoretical model including both effects is developed and is in agreement with the experimental data. Theoretical calculations indicate that high tuning efficiency and low tuning voltage can be achieved by expanding to the exchange spin wave regime or by utilizing compact on-chip magnonic waveguides. We anticipate that further scaling the YIG devices to the micro- and nano-scale would allow on-chip electric field control of spin waves. Our finding provides opportunities for direct electric tuning in YIG devices, which are widely used and indispensable for modern electronics.

This work is supported by the DARPA/MTO MESO program. H. X. T. acknowledges support from a Packard Fellowship in Science and Engineering. The authors thank Michael Power for assistance in device preparation and Dr. Changling Zou for helpful discussion.

\* michael\_flatte@mailaps.org

† hong.tang@yale.edu

- [1] Y. Kajiwara *et al.*, Nature **464**, 262 (2010).
- [2] B. Lenk, H. Ulrichs, F. Garbs, and M. Münzenberg, Phys. Rep. **507**, 107 (2011).
- [3] V. V. Kruglyak, S. O. Demokritov, and D. Grundler, J. Phys. D **43**, 264001 (2010).
- [4] A. Khitun, M. Bao, and K. L. Wang, J. Phys. D **43**, 264005 (2010).
- [5] E. G. Spencer, R. C. Lecraw, and A. M. Clogston, Phys. Rev. Lett. **3**, 32 (1959).
- [6] A. A. Serga, A. V. Chumak, and B. Hillebrands, J. Phys. D **43**, 264002 (2010).
- [7] O. Büttner, M. Bauer, S. O. Demokritov, B. Hillebrands, Y. S. Kivshar, V. Grimalsky, Y. Rapoport, and A. N. Slavin, Phys. Rev. B **61**, 11576 (2000).
- [8] A. N. Slavin and I. V. Rojdestvenski, IEEE Trans. Magn. **30**, 37 (1994).
- [9] M. Wu, P. Krivosik, B. A. Kalinikos, and C. E. Patton, Phys. Rev. Lett. **96**, 227202 (2006).
- [10] H. L. Wang, C. H. Du, Y. Pu, R. Adur, P. C. Hammel, and F. Y. Yang, Phys. Rev. Lett. **112**, 197201 (2014).
- [11] D. Qu, S. Y. Huang, J. Hu, R. Wu, and C. L. Chien, Phys. Rev. Lett. **110**, 067206 (2013).
- [12] J. Losby, Z. Diao, F. F. Sani, D. Grandmont, M. Belov, J. Burgess, W. Hiebert, and M. Freeman, Solid State Commun. (to be published).
- [13] J. Becker, F. Rödelberger, T. Weyrauch, H. Benner, W. Just, and A. Cénys, Phys. Rev. E **59**, 1622 (1999).
- [14] E. Padrón-Hernández, A. Azevedo, and S. M. Rezende, Appl. Phys. Lett. **99**, 192511 (2011).
- [15] P. Baettig and T. Oguchi, Chem. Mater. **20**, 7545 (2008).
- [16] S.-W. Cheong and M. Mostovoy, Nature Mater. **6**, 13 (2007).
- [17] C. Ederer and C. J. Fennie, J. Phys.: Condens. Matter **20**, 434219 (2008).



- [18] T. Kubacka *et al.*, Science **343**, 1333 (2014).
- [19] P. Rovillain *et al.*, Nature Mater. **9**, 975 (2010).
- [20] M. Bao *et al.*, Appl. Phys. Lett. **101**, 022409 (2012).
- [21] Y. K. Fetisov and G. Srinivasan, Appl. Phys. Lett. **93**, 033508 (2008).
- [22] I. V. Zavislyak, V. P. Sohatsky, M. A. Popov, and G. Srinivasan, Phys. Rev. B **87**, 134417 (2013).
- [23] I. V. Zavislyak, M. A. Popov, G. Sreenivasulu, and G. Srinivasan, Appl. Phys. Lett. **102**, 222407 (2013).
- [24] D. Awschalom and N. Samarth, Physics **2**, 50 (2009).
- [25] Z. Cao, X. Yu, and R. Han, Phys. Rev. B **56**, 5077 (1997).
- [26] I. Dzyaloshinsky, J. Phys. Chem. Solids **4**, 241 (1958).
- [27] T. Moriya, Phys. Rev. Lett. **4**, 228 (1960).
- [28] V. K. Dugaev, P. Bruno, B. Canals, and C. Lacroix, Phys. Rev. B **72**, 024456 (2005).
- [29] H.-B. Braun and D. Loss, Phys. Rev. B **53**, 3237 (1996).
- [30] Y. Aharonov and A. Casher, Phys. Rev. Lett. **53**, 319 (1984).
- [31] T. Liu and G. Vignale, Phys. Rev. Lett. **106**, 247203 (2011).
- [32] T. Liu and G. Vignale, J. Appl. Phys. **111**, 083907 (2012).
- [33] T. W. O’Keeffe and R. W. Patterson, J. Appl. Phys. **49**, 4886 (1978).
- [34] W. L. Bongianni, J. Appl. Phys. **43**, 2541 (1972).